J. Micromech. Microeng. **17** (2007) 1715–1720 doi:10.1088/0960-1317/17/8/039

A normally latched, large-stroke, inchworm microactuator*

Risaku Toda and Eui-Hyeok Yang[1]

Jet Propulsion Laboratory, California Institute of Technology, 4800 Oak Grove Drive, Pasadena, CA 91109, USA

E-mail: Risaku.Toda@jpl.nasa.gov

Received 30 March 2007, in final form 1 June 2007
Published 30 July 2007
Online at stacks.iop.org/JMM/17/1715

Abstract
This paper presents the successful demonstration of a large-stroke, high-precision inchworm microactuator. The actuator is capable of zero-power latching, or forcibly maintaining its position by using pre-stressed spring load. The actuator is driven by a combination of a PZT-stack actuator unit for slider thrust and electrostatic comb-drive units for slider grip. Incremental step size is precisely adjustable to the tens of nanometers level by controlling the PZT-stack actuator voltage. The observed minimum step size was 59 nm/cycle. Large stroke is obtained by repeating the operation sequence numerous times. A large-stroke actuation exceeding 600 μm has been demonstrated. There is no conceivable limit to the stroke except for the length of the slider and external load.

(Some figures in this article are in colour only in the electronic version)

1. Introduction

Future space missions will require very large aperture telescopes to meet expected light gathering and resolution requirements. These telescopes will consist of extremely large, lightweight optical mirrors, which might require a large number of actuators capable of correcting the mirror shapes. While mirror face sheet technology development has resulted in significant advances in lightweight optical quality face sheet materials, no comparable development has occurred in actuator technology development. The available actuators are still relatively heavy and bulky. To meet future requirements will require the development of large-stroke, precision, ultra-lightweight actuators that will match the needs and properties of future lightweight mirrors. Using a combination of ultra-lightweight microactuators (weighing only approximately 100 mg), an active mirror system can be designed to have very low areal density. For instance, extremely thin nanolaminate mirrors (with an areal density of <0.2 kg m^{-2} [2]) can be supported by flexure beams and microactuators, which are also ultra-lightweight, to meet the areal density requirements of future space telescope mirrors. Using even a hundred such microactuators per square meter would add only approximately 10 g m^{-2} to the mirror weight (excluding interconnecting wires and packaging).

An important requirement of the microactuators is the normally latched or zero-power latching scheme. Here, the zero-power latching refers to the capability that a moving part remains passively gripped at the same position when power (i.e. voltage) is off. The primary benefits of latching are power efficiency and robustness against power interruption. Other requirements for 'shape correction' of mirrors include a stroke of >1 mm and step resolution of <30 nm ($\lambda/20$ at $\lambda = 633$ nm), with an actuation force of a few tens of mN. Many MEMS-based inchworm actuators have been previously reported [3–15]; however, none appears to satisfy all the requirements stated above. A MEMS-based electrostatic inchworm motor previously reported [3] moves 400 μm stroke. However, the step size of this actuator is defined by the pitch of gear teeth (several μm) and it is too large for mirror shape correction applications. A mesoscale piezoelectric inchworm actuator [4] is heavy and bulky for the applications stated above. Inchworm actuators with thermal actuation [5–7] are undesirable for our applications. This is because thermally actuated devices suffer the risk of random actuation if ambient heating or cooling occurs, resulting in uncontrolled initiation of the actuation mechanism. A surface

* This paper was presented at the 19th IEEE MEMS Conference, held in Istanbul, Turkey, 22–26 January 2006, and is an expansion of the abstract as printed in the Technical Digest of the meeting [1].

[1] Present address: Stevens Institute of Technology, Hoboken, NJ 07030, USA.

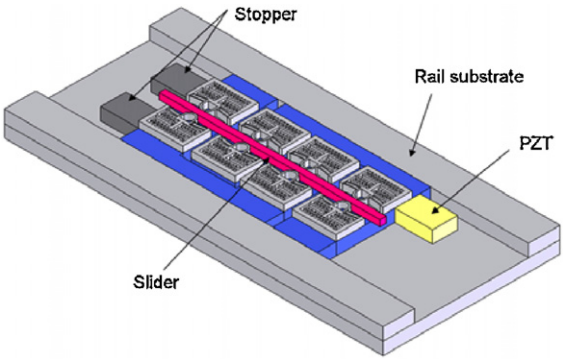

Figure 1. Actuator schematic. The actuator is driven by a combination of the electrostatic comb drive and PZT forces.

micromachined stepping actuator [8] offers 500 μN force, $\pm$100 μm travel and 10 nm step size, but the actuation force of a few tens of mN is required with a larger-actuator-stroke. Inchworm actuators using electrostatic clutching have been reported [2, 9, 10]. However, to our knowledge, none of the previous MEMS inchworm microactuators has demonstrated zero-power latching capability. We have previously attempted, unsuccessfully, to develop a latching-type actuator [16].

In this paper, we present a successful demonstration of a normally latched inchworm microactuator. This actuator is ultimately capable of large-stroke and high precision motion. The actuator in this paper has a single degree of freedom, which can be located and oriented in any desired direction in the future telescope mirror structures in space.

2. Design

Figure 1 shows the schematic of the inchworm actuator, consisting of a slider and two comb-drive units mounted on a rail substrate. The slider is inserted at the center trench and grasped by clutches. The actuator is driven by a combination of the electrostatic comb drive and PZT forces. Figure 2 illustrates the operation sequence of the actuator. Step (0) shows initial unpowered status. In step (1), the comb-drive unit A is released by powering the comb drive while the unit B remains clutched. In step (2), the unit B and the slider are laterally pulled towards the right by a PZT stack actuator. In step (3), the unit A is clutched while the unit B is released. In step (4), the unit B is pushed back by the PZT. One cycle of actuation yields a one step increment of slider motion towards the right. By repeating the actuation sequence for many times, large cumulative stroke is achieved. This sequence is reversible; therefore, the slider can be driven bidirectionally. The step increment resolution can be adjusted ultimately at the level of a few nanometers by controlling the voltage applied to the PZT stack. The intertwining U-letter-shaped comb-drive unit design is intended to enhance the stability of the slider motion. During the operation cycle, the slider is gripped by at least four clutches at a time. Also, the slider is confined to linear motions only, mitigating undesired slider tilt and drag friction. However, small drag friction may be induced when the slider is in contact with the underlying backbone structure and/or overlaying lid. This actuator is capable of zero-power latching, that is, the slider is gripped and its position is maintained when power is turned off. For this actuator, latching is made possible by pre-stressing tether beams during the assembly. Figure 3 illustrates the slider

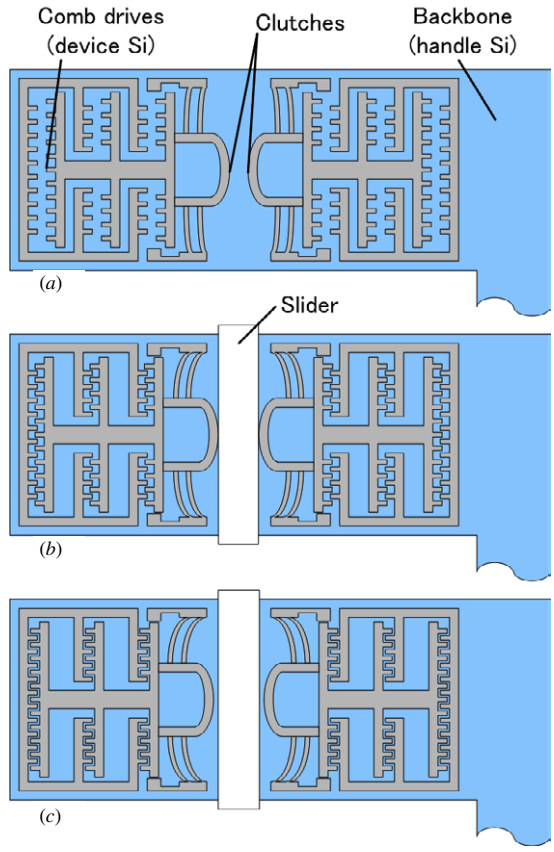

Figure 3. Slider insertion and comb-drive configuration. Opposing clutches and comb drives are fabricated on the 100 μm thick device layer of the SOI wafer, and the underlying 400 μm thick handle silicon is used as a backbone structure. (*a*) Comb gaps are wide (at least 5 μm spacing) before slider insertion, (*b*) comb gap width is reduced to approximately 1 μm and tether beams are pre-stressed after slider insertion, (*c*) comb-drive powered and clutches separated from the slider.

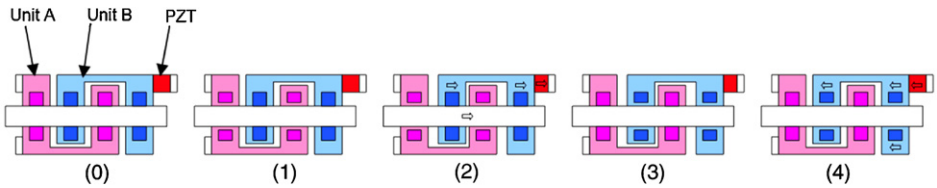

Figure 2. Operation sequence. (0) Unpowered latching mode, (1) unit A released, (2) unit B laterally moved to right, (3) unit A clutched, unit B released, (4) unit B moved back.

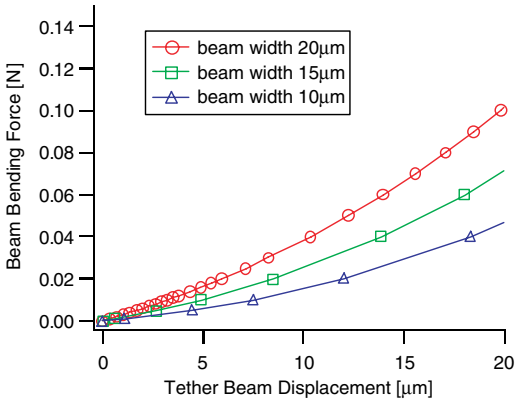

Figure 4. FEM analysis for tether beam displacement versus applied force. For a 10 μm wide tether beam, a displacement of 10 μm due to slider insertion results in a tether beam bending force of 20 mN, clamping the slider without supplying external power.

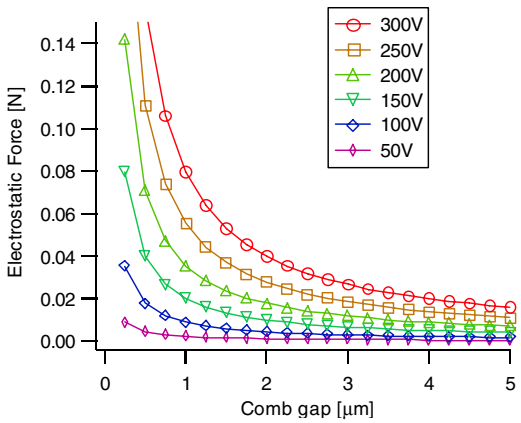

Figure 5. Estimated electrostatic force. For a comb-drive unit with a gap of 1 μm, powered by 200 V exerts a force of 40 mN, which overcomes the tether beam bending force of 20 mN, derived in figure 4, and therefore releases the slider.

insertion and tether beam pre-stressing scheme. The comb-drive unit is fabricated on a SOI wafer with a 100 μm thick device layer to increase both the stiffness and the electrostatic force. For processing this 100 μm thick layer, the aspect ratio limitation in the deep reactive ion etching (DRIE) process confines the trench width (comb gap) to be larger than roughly 5 μm. Therefore, the comb-drive structure is fabricated as 'unengaged' so that the initial gap between each comb tooth is a 5 μm gap, as shown in figure 3(*a*). The slider insertion allows the comb-drive teeth to get post-engaged as shown in figure 3(*b*), thereby narrowing the comb-tooth gap to approximately 1 μm. Also in figure 3(*b*), once the slider is inserted, tethers are displaced by approximately 10 μm and, therefore, grip the slider without external power since they are pre-stressed. By applying voltage to the comb drive, the clutches are electrostatically pulled away to release the slider (figure 3(*c*)). Figure 4 shows the FEM analysis results for the bending of the tether beams. The estimated bending force applied to the tethers—approximately 20 mN—as a clutch is displaced by 10 μm during the slider insertion process and bends the tether beam (figure 3(*b*)). On the other hand, the repulsion of the 10 μm wide tether beam perpetually pushes the slider with a force of 20 mN, as shown in figure 4. Figure 5 shows a plot of the estimated electrostatic force at the comb drives as a function of the comb gap. Before the slider insertion, the comb gap is approximately 5 μm and the electrostatic force is negligible. Once the slider is inserted, the comb gap narrows to approximately 1 μm (as depicted in figure 3(*b*)) and the electrostatic force is significantly increased. By applying 200 V to the comb drive, the estimated electrostatic force is approximately 40 mN, which exceeds the estimated tether bending force of 20 mN. Thus, the tethers are further bent by a few additional microns, so that the clutches are pulled away from the slider (figure 3(*c*)). Assuming that the static friction coefficient is 0.2 [17], each clutch can grip the slider with a force of up to 4 mN. In the power-off latching mode, four clutches on one side grip the slider with the force of 16 mN. This force can be significantly increased by adjusting the device layer thickness and the number of comb-drive columns and by surface coating on the slider to increase the friction coefficient. Three different tether beam widths (10, 15 and 20 μm) are tested. The devices with

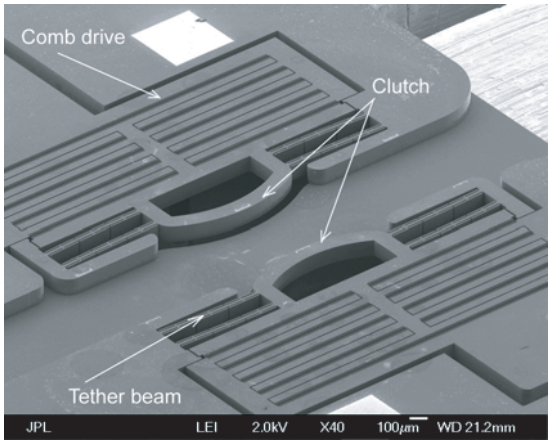

Figure 6. SEM image of the comb-drive unit. The comb-drive unit is prepared by performing DRIE on both sides of a SOI wafer.

narrow tether beams can be operated with smaller voltage, but the fabrication is difficult because the tether beam is relatively fragile. The devices with wider tether beams are more robust to fabricate, but they require higher voltage for the comb drive to overcome the tether beam restraining force. Past spacecrafts have successfully used high dc voltage (>100 V) on piezo actuators [18]. However, the use of high voltages on comb-drive actuators in space applications requires further thermal/vacuum environmental tests not addressed in this paper.

3. Fabrication

The inchworm actuator consists of two comb-drive units, a slider, a rail substrate and a PZT-stack actuator. Individual parts were fabricated separately and manually assembled. The comb-drive unit was made from a SOI wafer using DRIE on the both sides of the wafer. Clutches and comb drives are fabricated on the 100 μm thick device layer of the SOI wafer and the underlying 400 μm thick handle layer is used as a backbone structure. Figure 6 shows a SEM image of the comb-drive unit, consisting of clutches, tether beams and multiple

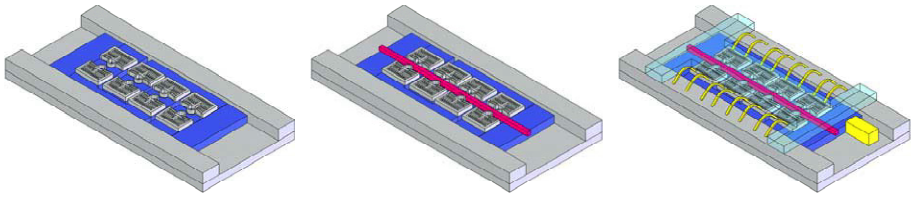

(*a*) (*b*) (*c*)

Figure 7. Assembly procedure of an inchworm actuator. (*a*) A pair of comb-drive units is placed on the rail. (*b*) The slider is inserted between clutches. (*c*) The PZT and the lid are attached by epoxy adhesive, followed by a wire-bonding process.

columns of comb drives. To control the sidewall profile of the tether beams during the DRIE process, H-shaped etch fin geometry was employed [19]. A rail substrate was made by attaching side-rails to the base plate by epoxy adhesive. The slider was fabricated by a slicing silicon wafer using a dicing saw. Therefore, the sidewall surface of the slider is slightly striated at an oblique angle. The surface of the slider was coated with a plasma enhanced chemical vapor deposition (PECVD) dielectric film to minimize sticking of the silicon slider to the silicon clutches. Figure 7 shows the assembly procedure of the inchworm actuator. After completing the fabrication of the actuator components, the driver units were mounted on the rail substrate (figure 7(*a*)). The slider was manually inserted between clutches using a probe needle (figure 7(*b*)). The striation of the slider sidewall seems to negatively impact the slider insertion yield due to nonuniform friction, which sometimes overstressed tether beam springs. The devices with wider tether beam widths are mechanically stronger and thus had better fabrication yield. After the slider insertion, the tether beams are displaced by approximately 10 μm and the slider is clamped by the tether beams. Finally, the PZT-stack actuator and a lid were attached using epoxy adhesive, and the assembled structure was wire-bonded (figure 7(*c*)). The stroke of the PZT actuator block with a dimension of 2.45 mm $\times$ 0.6 mm $\times$ 4 mm is >4 μm at 150 V. The role of the PZT actuator is to provide variable actuation steps of the comb-drive unit B (as shown in figure 2). Therefore, one end of the PZT is fixed to the comb-drive unit B while the opposite end is fixed to the underlying substrate. Figure 8 shows a microscope image of engaged comb teeth after the slider insertion. A side stopper was employed to limit the movement of the comb teeth in order to prevent mechanical damage. The side stopper and the moving part of the comb teeth were both electrically grounded to prevent pull-in contact and arc discharge. Figure 9 shows a fabricated inchworm actuator after the assembly and wire bonding. A PZT-stack actuator was epoxy mounted at one end of the driver unit. The other end of the driver unit was glued down to the rail substrate by epoxy adhesive. Figure 10 shows an actuator device that is capped with a silicon lid structure. This lid prevents the slider from accidentally popping out from clutches during testing.

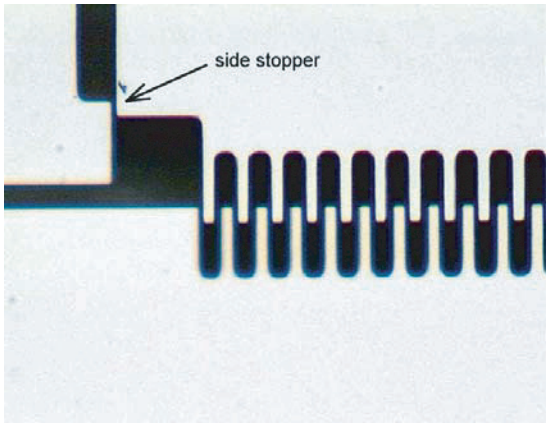

Figure 8. Microscope image of the comb drive and comb stopper. The comb stopper constraints the movements of the comb teeth and thus averts the comb-drive actuators from pull-in contact and arc discharge. The gap spacing at the side stopper is approximately 0.5 μm.

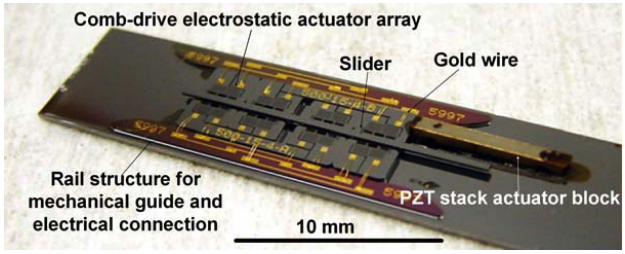

Figure 9. Image of an inchworm actuator after assembly and wire bonding.

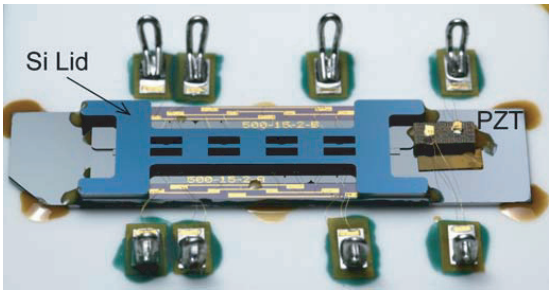

Figure 10. Image of an inchworm actuator mounted on a ceramic substrate for bench testing. The silicon lid prevents the slider from popping out.

4. Characterization

Before testing sequential operation, each comb-drive unit was tested by applying voltages under a microscope. As shown in figure 11, the comb drives started to pull the clutches away from the slider when a voltage exceeding 100 V was applied. The actuation test was performed with voltages equal to or less than 200 V applied to the comb drive. The tether beam widths of the tested devices are 15 μm. Devices with

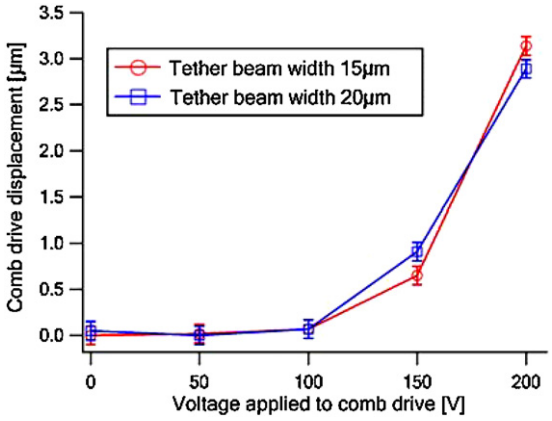

Figure 11. Measured comb-drive displacement versus applied voltage. Comb-drive actuators start to show displacement with dc voltage exceeding 100 V.

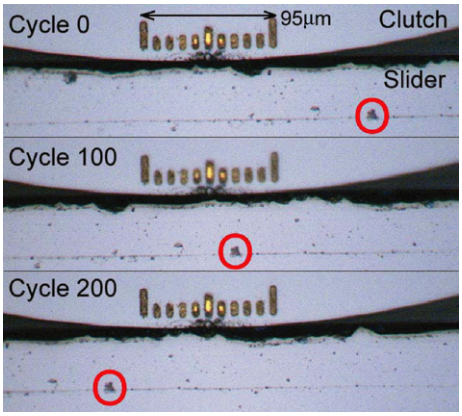

Figure 12. Microscope image during the sequential actuation test. The measured cumulative displacement after 200 cycles is approximately 178 μm.

10 μm width tether beams had a fabrication problem due to poor mechanical strength at the tether beam, while the devices with 20 μm width tether beams did not show clutch-releasing behavior due to insufficient comb-drive force with the 200 V dc voltage. Sequential actuator operation was tested using a LabVIEW-based set-up consisting of interfaced power relays and power supplies. Figure 12 shows captured microscope images during the sequential operation test. The voltages applied to the comb drive and the PZT-stack actuators were 200 V and 20 V, respectively. The measured cumulative stroke after 200-cycle actuation is 178 μm, with an operation speed of approximately 1 cycle per second. Figure 13 shows the measured slider displacement versus the number of cycles. The measured displacement is mostly linear with cycle counts. However, glitch was sometimes observed (not shown in figures) presumably due to the nonuniform friction caused by the dicing striation on the slider sidewall surfaces. The step size was varied by adjusting the PZT-stack actuator voltage. The measured incremental step size is approximately 59 nm/cycle, with the PZT-stack actuator voltage of 5 V; 384 nm/cycle, with 10 V, and 856 nm/cycle, with 20 V. The step size showed a tendency to be disproportional at lower PZT voltages probably due to PZT hysteresis and/or slider-drag friction.

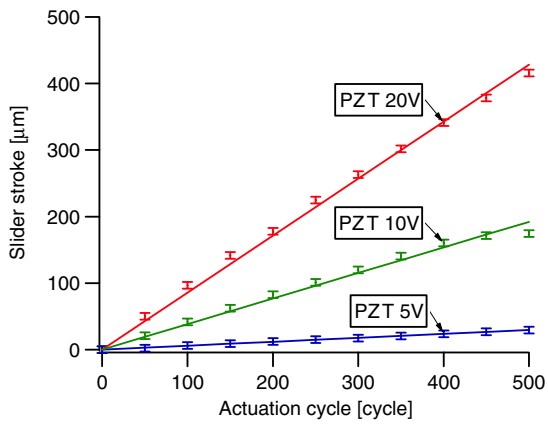

Figure 13. Actuation performance test. The measured total cumulative actuation during this test exceeded 600 μm.

5. Conclusions

We have successfully demonstrated the actuation of a normally latched, inchworm microactuator. Using a pre-stressed tether scheme, the microactuator is capable of maintaining its position when the power is cut off. The observed cumulative stroke exceeded 600 μm. A larger cumulative stroke can be easily achieved because, except for the length of the slider and applied load, there is no conceivable limit of the maximum stroke. Adjustment of the incremental step size as small as 59 nm/cycle was demonstrated by varying the PZT-stack actuator voltage. Further development is expected to analyze the actuator push force, to optimize the step size, to increase the operation speed, to improve linearity and to improve the packaging technique.

Acknowledgments

The authors would like to thank Dr Zensheu Zhang at the Jet Propulsion Laboratory for his support on the FEM analysis. The research described in this paper was carried out at the Jet Propulsion Laboratory, California Institute of Technology under a contract with the National Aeronautics and Space Administration. The research described here was performed under Research and Technology Development program at JPL.

References

[1] Toda R and Yang E-H 2006 Zero-power latching, large-stroke, high-precision linear microactuator for lightweight structures in space *IEEE MEMS 2006 (Istanbul, Turkey, 22–26 Jan)* pp 726–9

[2] Gullapalli S N, Yang E-H and Lih S-S 2003 New technologies for the actuation and control of large aperture lightweight optical quality mirrors *IEEE Aerospace Conf. (Big Sky, Montana)* vol 4 pp 1717–28

[3] Hollar S, Bergbreiter S and Pister K S J 2003 Bidirectional inchworm motors and two-DOF robot leg operation *12th Int. Conf. Solid State Sensors, Actuators and Microsystems (Boston)* pp 262–7

[4] Chen Q, Yao D J, Kim C J and Carman G P 1999 Mesoscale actuator device: micro interlocking mechanism to transfer macro load *Sensors Actuators* A **73** 30–6

[5] Okyar M 1997 Thermally excited inchworm actuators and stepwise micromotors: analysis and fabrication *Proc. SPIE* **3224** 372–9
[6] Pai M and Tien N C 1999 Current-controlled bi-directional electrothermally actuated vibromotor *Int. Conf. Solid-State Sensors and Actuators Transducers '99 (Sendai)* pp 1764–7
[7] Kwon H N, Jeong S H, Lee S K and Lee J H 2003 Design and characterization of a micromachined inchworm motor with thermoelastic linkage actuators *Sensors Actuators* A **103** 143–9
[8] de Boer M P, Luck D L, Ashurst W R, Maboudian R, Corwin A D, Walraven J A and Redmond J M 2004 High-performance surface-micromachined inchworm actuator *J. Microelectromech. Syst.* **13** 63–74
[9] Konishi S, Ohno K and Munechika M 2002 Parallel linear actuator system with high accuracy and large stroke *Sensors Actuators* A **97–98** 610–9
[10] Shutov M V, Howard D L, Sandoz E E, Sirota J M, Smith R L and Collins S D 2004 Electrostatic inchworm microsystem with long range translation *Sensors Actuators* A **114** 379–86
[11] Akiyama T and Shono K 1993 Controlled stepwise motion in polysilicon microstructures *J. Microelectromech. Syst.* **2** 106–10
[12] Matsubara T, Yamaguchi M, Minami K and Esashi M 1993 Stepping electrostatic microactuator *7th Int. Conf. Solid-State Sensors and Actuators Transducers '93 (Yokohama)* pp 50–3
[13] Lee A P, Nickel D J and Pisano A P 1993 Polysilicon linear vibromotors *7th Int. Conf. Solid-State Sensors and Actuators Transducers '93 (Yokohama)* pp 46–9
[14] Baltzer M, Kraus T and Obermeier E 1997 A linear stepping actuator in surface micromachining technology for low voltages and large displacements *Int. Conf. Solid-State Sensors and Actuators Transducers '97 (Chicago)* pp 781–4
[15] Tas N, Wissink J, Sander L, Lammerink T and Elwenspoek M 1998 Modeling, design and testing of the electrostatic shuffle motor *Sensors Actuators* A **70** 171–8
[16] Toda R and Yang E-H 2005 Development of latching type large vertical-travel microactuator *ASME InterPACK 2005 (San Francisco)*
[17] Hwang I H and Lee J H 2006 Novel measurement system of the friction coefficients for the DRIE sidewalls *IEEE MEMS 2006 (Istanbul)* pp 210–3
[18] Le Letty R, Barillot F, Fabbro H, Claeyssen F, Guay Ph and Cadiergues L 2004 Miniature piezo mechanisms for optical and space applications *9th Int. Conf. New Actuators Actuator 2004 (Bremen)* pp 177–80
[19] Grade J D, Jerman H and Kenny T W 2003 Design of large deflection electrostatic actuators *J. Microelectromech. Syst.* **12** 335–43